

The complex soft X-ray spectrum of NGC 4151

N. J. Schurch,^{1*} R. S. Warwick,² R. E. Griffiths¹ and S. M. Kahn³

¹*Department of Physics, Carnegie Mellon University, 5000 Forbes Avenue, Pittsburgh, PA 15213, USA*

²*Department of Physics and Astronomy, University of Leicester, University Road, Leicester LE1 7RH*

³*University of Columbia, Astrophysics Laboratory, 550 West 120th Street, New York, NY 10027, USA*

Accepted 2004 January 15. Received 2003 December 12; in original form 2003 March 24

ABSTRACT

We present a detailed analysis of the complex soft X-ray spectrum of NGC 4151 measured by the RGS instruments on board *XMM-Newton*. The *XMM-Newton* RGS spectra demonstrate that the soft X-ray emission is extremely rich in X-ray emission lines and radiative recombination continua (RRC), with no clear evidence for any underlying continuum emission. Line emission and the associated RRC are clearly detected from hydrogen-like and helium-like ionization states of neon, oxygen, nitrogen and carbon. The measured lines are blueshifted with a velocity of $\sim 100\text{--}1000\text{ km s}^{-1}$, with respect to the systemic velocity of NGC 4151, approximately consistent with the outflow velocities of the absorption lines observed in the ultraviolet spectrum of NGC 4151 by Kriss et al. in the mid-1990s, suggestive of an origin for the ultraviolet and soft X-ray emission in the same material. Plasma diagnostics from the observed helium-like triplets imply a range of electron temperatures of $\sim (1\text{--}5) \times 10^4\text{ K}$ and electron densities of between 10^8 and 10^{10} cm^{-3} . The soft X-ray spectrum of NGC 4151 is extremely similar to that of NGC 1068, in terms of both the atomic species present and the relative strengths of the observed emission lines and RRC (reported recently by Kinkhabwala et al.), suggesting that the soft X-ray excesses observed in many type 2 Seyfert galaxies may be composed of similar emission features. Modelling the RGS spectra in terms of emission from photoionized and photoexcited gas in an ionization cone reproduces all of the hydrogen-like and helium-like emission features observed in the soft X-ray spectrum of NGC 4151 *in detail* and confirms the correspondence between the soft X-ray emission in NGC 4151 and 1068. NGC 4151 shows somewhat lower individual ionic column densities than those measured for NGC 1068, indicating that the material in the ionization cones of NGC 4151 may be somewhat more dense than the material in the ionization cones of NGC 1068.

Key words: galaxies: active – galaxies: individual: NGC 4151 – galaxies: Seyfert – X-rays: galaxies.

1 INTRODUCTION

Prior to the advent of *XMM-Newton* and *Chandra*, the origin of the soft X-ray emission from heavily obscured active galactic nuclei (AGN) remained very uncertain. Recently, however, observations with *XMM-Newton* and *Chandra* have revolutionized our understanding of heavily obscured AGN [for a complete description of *XMM-Newton*, *Chandra* and their relative capabilities, see Jansen et al. (2001) and Weisskopf et al. (2002) and references therein]. The combination of the high spatial resolution afforded by *Chandra*, the large collecting area of *XMM-Newton* and the high spectral resolution X-ray spectroscopy capabilities (in the form of X-ray grating and CCD instruments) of both missions across the 0.1–12 keV band

is beginning to reveal many new details of the X-ray emission from heavily obscured AGN, particularly with regard to the soft X-ray emission from these objects. *Chandra* observations of several heavily obscured AGN have revealed considerable extended soft X-ray emission in each source, which is tightly correlated with the [O III] ($\lambda 5007$) emission observed with the *Hubble Space Telescope* (*HST*; NGC 1068, Young, Wilson & Shopbell 2001; Mrk 3, Sako et al. 2000; NGC 4151, Ogle et al. 2000; Circinus, Sambruna et al. 2001). In several of these sources (e.g. NGC 1068, Young et al. 2001), the extended X-ray emission and the [O III] ($\lambda 5007$) emission clearly trace the spiral arms and other large-scale structures out to a considerable distance from the active nucleus of the galaxy. Similarly, recent spectral observations of these AGN with the X-ray grating instruments on board *Chandra* (NGC 1068, Brinkman et al. 2002; Ogle et al. 2003; Mrk 3, Sako et al. 2000; NGC 4151, Ogle et al. 2000; Circinus, Sambruna et al. 2001) and *XMM-Newton*

*E-mail: schurch@andrew.cmu.edu

(Kinkhabwala et al. 2002) have revealed soft X-ray spectra dominated by prominent emission lines from a range of light elements (e.g. C, N, O, Ne, etc.). These observations constitute a growing body of evidence that suggests that the soft X-ray emission from heavily obscured Seyfert galaxies is largely composed of soft X-ray emission lines that originate in gas that is photoionized (and photoexcited) by the central AGN.

The type 1.5 Seyfert galaxy NGC 4151 was identified as an X-ray source over 30 years ago (Gursky et al. 1971). One of the brightest AGN accessible in the X-ray band, NGC 4151 has been extensively studied by missions such as *EXOSAT*, *Ginga*, *ROSAT*, *ASCA*, *CGRO* and more recently *RXTE*, *BeppoSAX*, *Chandra* and *XMM-Newton*. This observational focus has revealed that the spectrum of NGC 4151 from 0.1 to 100 keV comprises a complex mixture of emission and absorption components, probably originating in a variety of locations from the innermost parts of the putative accretion disc in NGC 4151, out to the extended narrow-line region (ENLR) of the galaxy. Despite the relatively poor quality of the spectra, previous observations (particularly observations with *ASCA*) did tentatively reveal several unresolved soft X-ray features, suggesting that the soft X-ray emission was somewhat more complex than had been previously suggested. The most prominent feature found with *ASCA* was at an energy of ~ 0.88 keV and was tentatively associated with O VIII Ly α radiative recombination continua (RRC) (Weaver et al. 1994; Griffiths et al. 1998). The detailed nature of the soft X-ray emission in NGC 4151 has only recently been revealed through a *Chandra* HETG observation (Ogle et al. 2000; Yang, Wilson & Ferruit 2001). This observation demonstrated that the soft X-ray spectrum was composed almost entirely of emission lines and RRC, with little or no detected continuum emission of any form (and hence no absorption features). Utilizing the excellent spatial resolution of *Chandra*, Ogle et al. (2000) resolved ~ 70 per cent of the soft X-ray emission as extended emission, originating up to 11.5 arcsec from the AGN, which demonstrated an excellent correspondence with the biconical [O III] ($\lambda 5007$) emission previously imaged with the *HST* (Evans et al. 1993). The *Chandra* observation was even capable of resolving the spatial profiles of several of the brightest emission lines (including the iron K α emission line), showing that the individual line emission was genuinely extended along the direction of the optical ionization cones. The *Chandra* observation dramatically confirmed that the hard X-ray spectrum of NGC 4151 is strongly cut off below 2 keV and that the soft excess is not predominantly produced by electron scattering of the hard X-ray continuum. The *Chandra* analysis finds evidence for both photoionized and collisionally ionized (thermal) gas in the ENLR. However, many of the details of the ionized medium remained elusive, as a result of the large number (33 in total) and low significance of the features detected.

This paper is organized as follows. Section 2 details the *XMM-Newton* observations of NGC 4151. Section 3 presents the *XMM-Newton* RGS spectra and discusses the spectral modelling in terms of emission from an ionization cone. Section 4 compares the RGS spectra of NGC 4151 with the soft X-ray spectra of NGC 1068 and Mrk 3. Section 5 presents a preliminary look at the correspondence between the *XMM-Newton* RGS and the *XMM-Newton* EPIC soft X-ray spectra of NGC 4151.

2 THE *XMM-NEWTON* OBSERVATIONS

NGC 4151 was observed with *XMM-Newton* five times during 2000 December 21–23. The RGS instruments were active for all five observations and the data were processed with the standard RGS pipeline processing chains incorporated in the *XMM-Newton* SAS

v5.4.1. Dispersed source spectra and background spectra were extracted with the automated RGS extraction tasks in the SAS. The SAS filters the RGS events in dispersion channel versus CCD pulse height space to separate the data from the different spectral orders. Investigation of the individual spectra indicate that the second-order RGS spectra contain a negligible amount of information (a count rate of ≤ 10 per cent of that in the first-order spectra, despite having ~ 60 per cent of the effective area below 10 Å) and as a result only the first-order spectra are presented here. The resulting spectra have a total effective exposure time of ~ 128 ks and ~ 125 ks for the RGS 1 and 2 instruments respectively. A previous investigation of the *XMM-Newton* EPIC spectra confirms that the soft X-ray spectrum of NGC 4151 remained relatively constant for the duration of the observation (Schurch et al. 2003). The spectra from the five observations were co-added to produce a single high signal-to-noise ratio source spectrum and a single background spectrum for each RGS instrument. The full spectra and individual lines were analysed with both maximum-likelihood and χ^2 minimization techniques. For the maximum-likelihood analysis the spectra were left unbinned; however, for the χ^2 minimization techniques (which, in general, are not particularly well suited to fitting the sharp features observed in this and similar high-resolution soft X-ray spectra), the spectra were binned to a minimum of 20 counts per spectral channel. Investigation of the spatial extent of the X-ray emission observed by *XMM-Newton* reveals that the soft X-ray emission is not significantly extended on scales greater than the mirror point spread function (PSF), consistent with the details of the previously reported *Chandra* observation of NGC 4151 (Ogle et al. 2000).

3 MODELLING THE RGS SPECTRA

Fig. 1 shows the *XMM-Newton* RGS spectra from the combined observations of NGC 4151. The spectrum is completely dominated by line emission and RRC. Line emission is clearly detected from hydrogen-like and helium-like ionization states of neon, oxygen, nitrogen and carbon, and in many cases the line emission associated with these ions is not limited to the Ly α (2p–1s) transition but includes higher-order resonance transitions (np –1s) labelled β – ϵ for the different hydrogen-like and helium-like species respectively. Much of the unidentified line emission below ~ 16 Å can be associated with a multitude of unresolved iron L-shell emission lines, along with some contribution from hydrogen-like and helium-like silicon and magnesium. The spectra show no significant continuum emission and no fluorescent line emission. (There may be a marginal detection of silicon K α fluorescence at ~ 7.1 Å. However, without a good knowledge of the iron L-shell emission in this region, it is not possible to measure the line cleanly.)

3.1 The emission lines

The spectrum is remarkably similar to the soft X-ray spectrum of the archetypal bright type 2 Seyfert galaxy NGC 1068, reported by Kinkhabwala et al. (2002). Both sources show strong emission-line triplets from helium-like nitrogen and oxygen, with a similar pattern of resonance, intercombination and forbidden linestrengths. Following the analysis of the *XMM-Newton* RGS observation of NGC 1068 presented in Kinkhabwala et al. (2002), line fluxes, centroid energies and linewidths were determined for the bright, unambiguously identified, emission lines observed in the spectra. The spectral fits quoted here for individual strong line features were performed with χ^2 minimization techniques (and correspondingly the data were binned to a minimum of 20 counts per spectral channel). An examination of

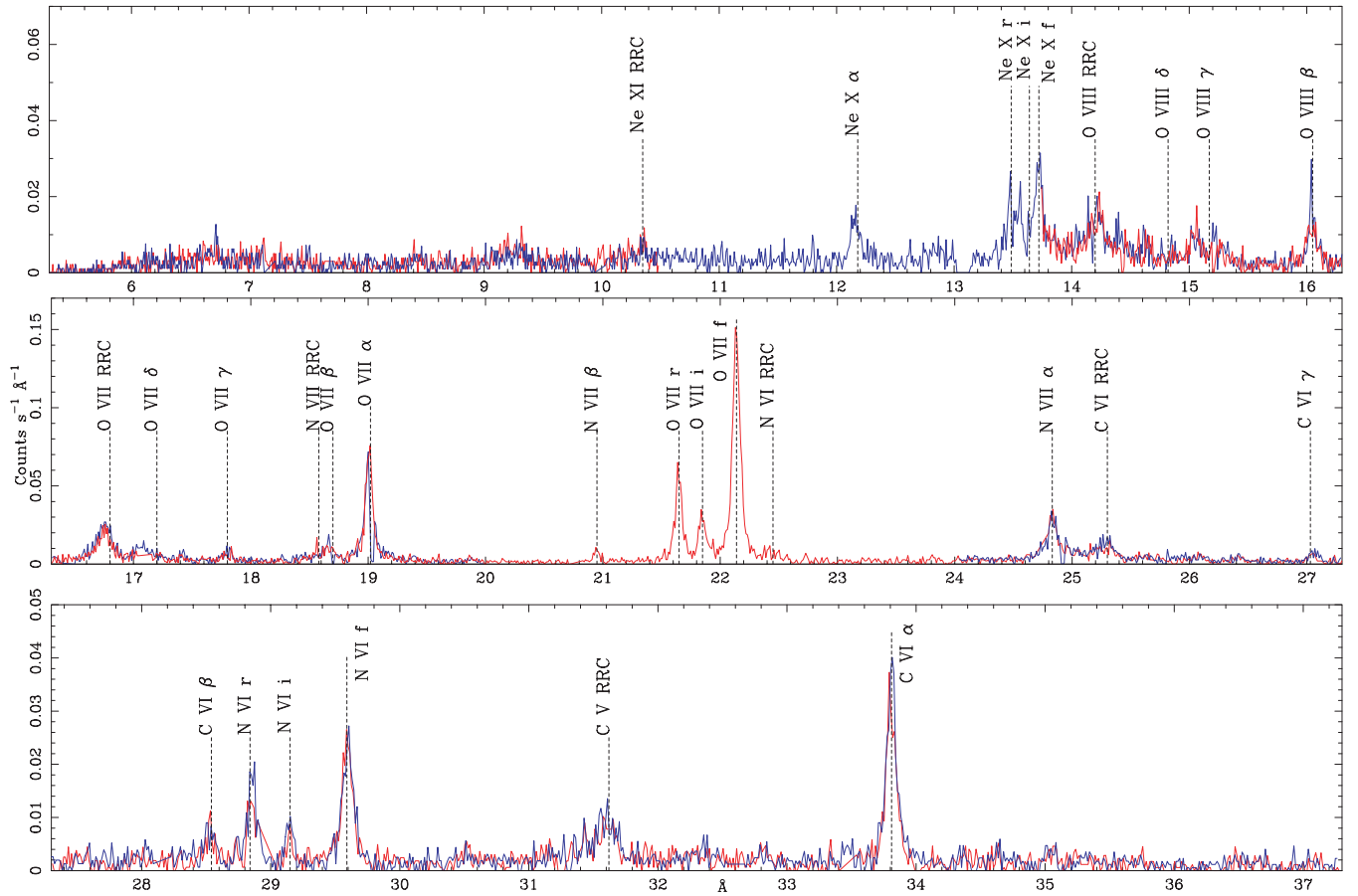


Figure 1. RGS 1 (red) and RGS 2 (blue) spectra of NGC 4151. The spectra here are unbinned. Spectral discontinuities are caused by chip gaps in the CCD arrays and the effects of the damaged RGS CCDs. Unambiguously identified hydrogen-like and helium-like emission lines are labelled along with the clearly identified RRC.

the fit properties using maximum-likelihood fitting techniques for individual lines reveals that the best-fitting parameters are not significantly different using these statistical techniques in comparison with the χ^2 fits, as expected given the bright nature of the features examined here. The intrinsic profiles of the emission lines are represented by a line model with a Gaussian profile (we caution, however, that the original line profile may in fact not be Gaussian, although it does appear to be a good approximation for the lines presented here), which allows the determination of accurate line centroid energies, fluxes and, in some cases, linewidths. The results of fitting this profile to the brightest emission lines are given in Table 1.

The measured fluxes take account of the Galactic column density ($2.1 \times 10^{20} \text{ cm}^{-2}$; Warwick, Done & Smith 1995) using the *tbabs* model in *XSPEC*, and the line shifts are measured with respect to the source redshift of $z = 0.00332$. The systematic uncertainty on measuring the centroid line energies of the lines is estimated to be $\sim 8 \times 10^{-3} \text{ \AA}$ (which corresponds to about 150 km s^{-1} ; *XMM* Users Handbook v2.1, 2002). The quoted errors are 90 per cent confidence levels as defined by a $\Delta\chi^2 = 2.71$ criterion (i.e. assuming one parameter of interest) and include the systematic uncertainty added in quadrature. Most of the measured line centroid energies are consistent with a mild blueshift, of between ~ 100 and 1000 km s^{-1} , with respect to the systemic velocity of the lines. This implies a line-of-sight outflow velocity for the ionized material of $\lesssim 1000 \text{ km s}^{-1}$, consistent with the line shifts of the absorption lines observed in the ultraviolet (UV) spectrum of NGC 4151 ($\sim 600 \text{ km s}^{-1}$; Kriss

et al. 1995). Many of the observed linewidths are largely unconstrained, with the spectral fitting only yielding upper limits (these are not quoted in Table 1); however, the seven linewidths that are constrained by the spectral fitting appear to show a bimodal distribution, with the shorter-wavelength lines having an average linewidth of $\sigma \sim 0.025 \text{ \AA}$ (1000 km s^{-1} full width at half-maximum, FWHM) and the longer-wavelength lines having an average linewidth of $\sim 0.005 \text{ \AA}$ ($\sim 200 \text{ km s}^{-1}$ FWHM). The observed linewidths imply that the intrinsic velocity dispersion of the outflowing material is $\lesssim 1000 \text{ km s}^{-1}$, which is somewhat lower than the linewidths of the absorption lines observed in the UV ($1000\text{--}2500 \text{ km s}^{-1}$; Kriss et al. 1995). The bimodal distribution of the linewidths as a function of the wavelength of the line is suggestive of a scenario in which individual clouds of emitting material close to the source of the ionizing continuum are moving more rapidly than clouds further from the continuum source. The large majority of the soft X-ray flux of NGC 4151 as measured by *Chandra* is not extended on scales larger than ~ 2 arcsec, demonstrating that the reported extended soft X-ray flux will not contribute considerably to the linewidths measured in the RGS spectrum.

3.2 Temperature diagnostics with radiative recombination continua

The RRC identified in the RGS spectra are the result of a free electron recombining directly into a bound state of an ion.

Table 1. Line properties of individual emission lines observed in the RGS spectra of NGC 4151.

Line ID	λ_{obs} (Å)	λ_{rest}^a (Å)	Line shift (km s ⁻¹)	σ_{obs} ($\times 10^{-2}$ Å)	Flux ($\times 10^{-4}$ photon s ⁻¹ cm ⁻²)
Ne X α	12.13 ^{+0.01} _{-0.01}	12.134	-120 ⁺²⁵⁰ ₋₂₅₀	2.6 ^{+1.0} _{-0.9}	0.42 ^{+0.05} _{-0.05}
Ne IX r	13.43 ^{+0.02} _{-0.01}	13.447	-430 ⁺⁴⁹⁰ ₋₂₆₀	2.4 ^{+1.9} _{-1.1}	0.47 ^{+0.05} _{-0.05}
Ne IX i	13.53 ^{+0.01} _{-0.02}	13.550	-470 ⁺²⁴⁰ ₋₃₄₀	2.0 ^{+1.6} _{-1.2}	0.46 ^{+0.15} _{-0.07}
Ne IX f	13.68 ^{+0.01} _{-0.02}	13.697	-310 ⁺²²⁰ ₋₁₈₀		1.03 ^{+0.1} _{-0.09}
O VIII β	16.00 ^{+0.02} _{-0.02}	16.006	-150 ⁺²³⁰ ₋₂₃₀	3.1 ^{+0.6} _{-0.6}	0.37 ^{+0.04} _{-0.04}
O VIII α	18.96 ^{+0.01} _{-0.01}	18.969	-210 ⁺¹³⁰ ₋₁₃₀		1.60 ^{+0.10} _{-0.10}
O VII r	21.59 ^{+0.01} _{-0.01}	21.603	-230 ⁺¹⁴⁰ ₋₁₄₀		1.19 ^{+0.09} _{-0.09}
O VII i	21.79 ^{+0.01} _{-0.01}	21.798	-230 ⁺¹²⁰ ₋₁₃₀		0.75 ^{+0.07} _{-0.07}
O VII f	22.08 ^{+0.01} _{-0.01}	22.101	-300 ⁺¹¹⁰ ₋₁₁₀	0.68 ^{+0.09} _{-0.09}	3.89 ^{+0.17} _{-0.19}
N VII β	20.89 ^{+0.01} _{-0.01}	20.910	-230 ⁺¹⁶⁰ ₋₁₅₀	0.7 ^{+0.5} _{-0.4}	0.22 ^{+0.04} _{-0.04}
N VII α	24.77 ^{+0.01} _{-0.01}	24.781	-190 ⁺¹¹⁰ ₋₁₁₀		0.81 ^{+0.09} _{-0.08}
N VI r	28.75 ^{+0.01} _{-0.01}	28.792	-350 ⁺¹¹⁰ ₋₁₁₀		0.45 ^{+0.07} _{-0.06}
N VI i	29.09 ^{+0.02} _{-0.02}	29.075	30 ⁺²⁵⁰ ₋₁₆₀		0.36 ^{+0.06} _{-0.06}
N VI f	29.51 ^{+0.01} _{-0.01}	29.531	-290 ⁺¹⁰⁰ ₋₁₁₀		1.15 ^{+0.12} _{-0.12}
C VI β	28.43 ^{+0.01} _{-0.01}	28.466	-390 ⁺¹³⁰ ₋₁₃₀	0.9 ^{+0.3} _{-0.3}	0.37 ^{+0.05} _{-0.05}
C VI α	33.69 ^{+0.01} _{-0.01}	33.736	-440 ⁺⁹⁰ ₋₉₀		1.79 ^{+0.16} _{-0.16}

^aVainshtein & Safronova (1978).

Recombination to the ground state represents the dominant transition and is the only transition considered during the spectral modelling. The free electrons can have any energy above the recombination threshold and hence the feature produced is neither symmetrical nor narrow. The energy of the electrons prior to the recombination process is dependent upon the electron temperature of the emitting plasma, and hence the width of the RRC features provides a direct measurement of the recombining electron temperature, T_e (Liedahl & Paerels 1996; Liedahl 1999). RRC originating in hot plasmas are broad and often subtle features; however, RRC from cool plasmas are narrow, prominent, features. The velocity dispersion of the emitting material will affect the RRC in exactly the same manner as it affects the emission lines discussed previously, but this effect is negligible here because of the low velocities of the ions involved compared to that of the electrons. RRC from hydrogen-like and helium-like ionization states of Ne, O, N and C are clearly identifiable in Fig. 1. Electron temperatures were determined for the bright, unambiguously identified, RRC (Table 2) using the RRC profiles generated by the ‘ionization cone’ model discussed in Section 3.4 fitted, using χ^2 minimization techniques, to the individual RRC. Again, an examination of the fit properties using maximum-likelihood fitting techniques for individual features reveals that the best-fitting parameters are not significantly different using these statistical techniques in comparison with the χ^2 fits. The derived electron temperatures imply electron temperatures of $\sim(2-4) \times 10^4$ K. The association of high-ionization emission lines (e.g. O VIII, Ne X, etc., identified in the previous section) with such a low-temperature plasma is strongly indicative of a plasma whose ionization state is governed by photoionization as opposed to collisional ionization.

Table 2. Electron temperatures from RRC.

RRC	T_e (eV)
C V	2.5 ^{+1.5} _{-0.5}
C VI	4.0 ^{+1.0} _{-1.0}
N VI	3.0 ^{+3.0} _{-1.0}
N VII	4.0 ^{+2.0} _{-1.5}
O VII	4.0 ^{+0.5} _{-0.5}
O VIII	6.0 ^{+1.0} _{-2.0}

Table 3. Helium-like triplet plasma diagnostic ratios.

Triplet ID	R	G
Ne IX	2.3 ^{+0.7} _{-0.7}	3.2 ^{+1.2} _{-0.9}
O VII	3.4 ^{+0.4} _{-0.3}	3.9 ^{+0.5} _{-0.5}
N VI	3.0 ^{+1.1} _{-0.8}	3.4 ^{+1.0} _{-0.8}

3.3 Plasma diagnostics with helium-like triplets

The three most prominent X-ray emission lines from helium-like ions correspond to transitions from the $n = 2$ shell to the $n = 1$ shell and are the resonance ($1s2p \ ^1P_1 \rightarrow 1s^2 \ ^1S_0$), the intercombination ($1s2p^3 \ P_{2,1} \rightarrow 1s^2 \ ^1S_0$) and the forbidden ($1s2s \ ^3S_1 \rightarrow 1s^2 \ ^1S_0$) line transitions (Pradhan, Norcross & Hummer 1981). Ratios of the measured line fluxes for the recombination, intercombination and forbidden lines from helium-like ions provide a diagnostic of the electron density and temperature in hot plasmas. Gabriel & Jordan (1969) were the first to recognize the importance of the helium-like triplet lines and used linestrength ratios to analyse the solar corona spectra in detail. The ratio of the intensity of the forbidden line to the intensity of the intercombination line (R , where $R = f/i$) is sensitive to the electron density of the plasma, and the ratio of the sum of the intensities of the forbidden and intercombination lines to the intensity of the resonance line [G , where $G = (i + f)/r$] is sensitive to the electron temperature of the plasma. For a detailed discussion of the manner in which the ratios depend on the electron density and the plasma temperature, see Pradhan et al. (1981), Porquet & Dubau (2000) and Porquet et al. (2002) and references therein.

The R and G ratios for the Ne, O and N triplets observed in the RGS spectrum of NGC 4151 are given in Table 3. The G -values imply an electron temperature of $\lesssim 10^5$ K, consistent with the electron temperatures implied from the properties of the observed RRC and consistent with photoionization being the dominant ionization mechanism in the plasma (Porquet & Dubau 2000). The R -values imply electron densities of $\sim 10^8-10^9$ cm⁻³ in nitrogen and oxygen and $\sim 10^{10}-10^{11}$ cm⁻³ in neon (Porquet & Dubau 2000). In particular, the ratios calculated from the oxygen triplet (which is both the strongest and the least confused of the helium-like triplets) strongly imply a photoionized plasma. However, extracting detailed values of density and temperature for the emitting material is complicated by the possibility that a strong radiation field (i.e. photoexcitation) can mimic the effect that a relatively high density has on the linestrengths. In such a situation, the electron density and, to a lesser extent, the electron temperature can be overestimated (Porquet et al. 2002). We note that the expected contribution of blended dielectronic satellite lines to these ratios has not been taken into

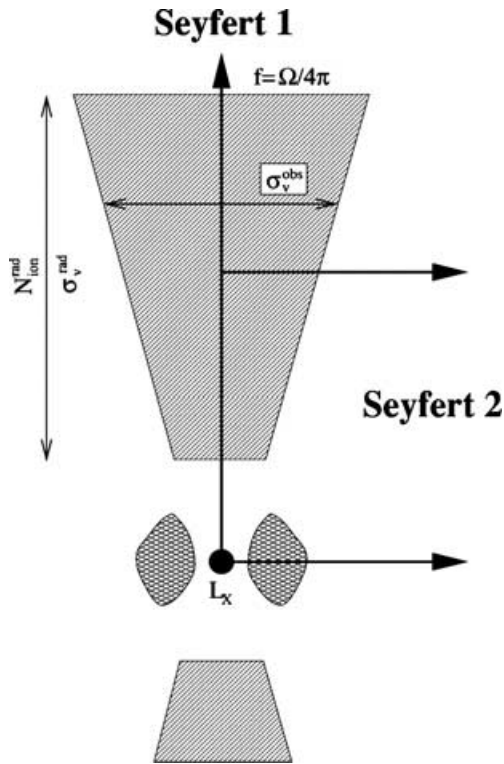


Figure 2. Schematic cartoon of the ‘ionization cone’ model (not to scale). The central nuclear components (black hole and accretion disc), denoted by the black spot, are surrounded by a dense absorbing torus of neutral dust and gas. The optically thin material perpendicular to the plane of the absorbing torus sees the direct continuum from the X-ray source and becomes strongly ionized, forming ionization cones. The line emission from these cones is observable from type 2 Seyfert galaxies due to the suppression of the direct continuum, whereas the ionization cones in type 1 Seyfert galaxies are only seen through their absorption of the direct continuum (Kinkhabwala et al. 2002).

account in the values quoted here. For the N and O triplets this contribution is negligible; however, the Ne triplet is significantly affected. For a high-temperature, collisionally dominated plasma, the additional contribution can result in an error of ~ 1 per cent and ~ 9 per cent for the *R* and *G* ratios, respectively. However, for a photoionized plasma, where the temperatures are several orders of magnitude lower, this effect can be considerably greater (Porquet et al. 2002).

3.4 The ionization cone model

Given the similarity between the RGS spectra of NGC 1068 and 4151, we utilize the ‘ionization cone’ model developed by Kinkhabwala et al. (2002) in their analysis of the RGS spectrum of NGC 1068, to fit the RGS spectrum of NGC 4151. This model, which was incorporated into XSPEC for ease of spectral fitting, reproduces the hydrogen-like and helium-like line emission, and the associated RRC, from an irradiated cone of optically thin plasma (cf. the ionization cones observed in [O III] by *HST*) shown schematically in Fig. 2. The model includes the effects of both photoionization and, crucially, photoexcitation. Photoexcitation is the process by which the absorption of a photon with insufficient energy to ionize the atom results in the transition of an inner-shell electron

to a higher energy level within the atom. The excited electron will rapidly undergo one or more radiative transitions, decaying back to its original energy state. For each atomic species, photoexcitation is expected to enhance the intensity of the higher-order resonance transition lines relative to the first-order resonance line. Photoexcitation was observed to play a significant role in the spectrum of NGC 1068, where the Ly β , Ly γ and Ly δ lines were significantly stronger than predicted by models based on pure photoionization or collisional ionization.

Here, as with NGC 1068, the plasma is irradiated by the unabsorbed intrinsic power-law continuum, the slope of which in the case of NGC 4151 is fixed at $\Gamma = 1.65$, based on the analysis of the hard X-ray *XMM-Newton* EPIC spectrum presented in Schurch et al. (2003). The luminosity of the central source, L_X , and the covering fraction of the cone, f , are fixed at $L_X = 6 \times 10^{43}$ erg s $^{-1}$ and $f = 0.1$, respectively. The modelling includes both Galactic column density (2.1×10^{20} cm $^{-2}$; Warwick et al. 1995) using the tbabs model in XSPEC and a source redshift of $z = 0.00332$. The electron temperatures for each atomic species were fixed at the temperatures found from the analysis of the RRC (Table 2), where possible, and the remaining RRC temperatures were fixed at the temperatures identified for NGC 1068 by Kinkhabwala et al. (2002) – based on the similarity between the observed bright RRC in NGC 4151 and the corresponding RRC in NGC 1068. The remaining free parameters of the model are the transverse velocity distribution of the lines, σ_v^{obs} , the radial velocity distribution of the lines, σ_v^{rad} , and the radial column density of each individual atomic species, N_{ion}^{rad} . The modelling presented in the next section includes a significant contribution from iron L-shell emission lines. Iron L-shell emission, known to be present in the soft X-ray spectrum of both Mrk 3 and NGC 1068, will contribute significantly between ~ 9 and 16 \AA (0.75–1.4 keV) and will result in an artificially high measure of the ionic column densities of neon and magnesium if it is not incorporated in the modelling.

3.5 Fitting the ionization cone model to the RGS spectra

The ionization cone model was fitted to the RGS spectra in XSPEC for simplicity. We note that the χ^2 minimization techniques, used earlier in the paper to fit specific bright spectral features, are, in general, not well suited to fitting wide-band X-ray grating spectra, which often incorporate many additional low-significance spectral features. With this in mind, the ionization cone model is fitted to the RGS spectra of NGC 4151 using maximum-likelihood fitting techniques. The complexity of this specific model makes the accurate determination of individual parameter errors problematic. Despite this caveat, the model provides a ‘good fit’ to all the hydrogen-like and helium-like line emission and RRC observed in the RGS spectra. Here, the term ‘good fit’ refers only to a set of parameters that correctly reproduces the distinct features observed in the spectrum (i.e. it is not a statistical measure of the goodness of fit of the model). Because of this, statistical errors are not quoted for either the column densities or the velocity measurements. Fig. 3 shows the best fit of the ionization cone model to all the hydrogen-like and helium-like emission lines and RRC in the RGS spectrum of NGC 4151. The best-fitting radial ionic column densities and the associated RRC electron temperatures are given in Table 4; σ_v^{obs} has a best-fitting value of ~ 400 km s $^{-1}$ and σ_v^{rad} has a best-fitting value of ~ 330 km s $^{-1}$. We do not quote any specific best-fitting values for the ionic column densities of iron responsible for the iron L-shell emission (Fe XVI–XXIII) owing to the unresolved nature of the specific iron

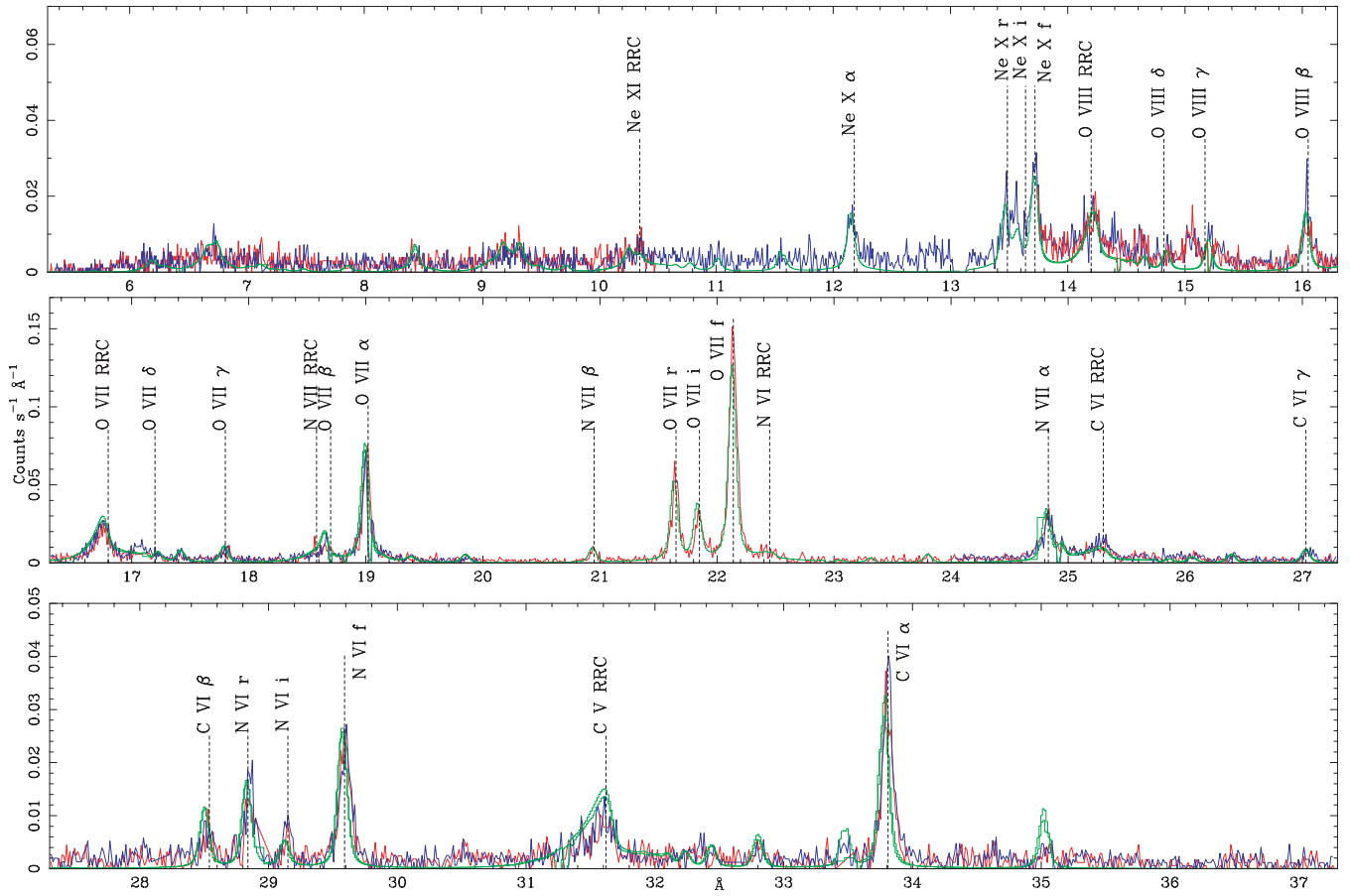


Figure 3. Best fit of the ionization cone model to the RGS spectra of NGC 4151. The unbinned RGS 1 and RGS 2 spectra are shown in red and blue along with the best-fitting model in green. The best-fitting model parameters are given in Table 4. Unambiguously identified hydrogen-like and helium-like emission lines and RRC are labelled in a similar fashion to that in Fig. 1.

Table 4. Best-fitting parameters for the ‘ionization cone’ model fit to the RGS spectra of NGC 4151.

Ion	$N_{\text{ion}}^{\text{rad}}$ (cm^{-2})	kT_e (eV)
C v	2.9×10^{17}	2.5
C vi	4.0×10^{17}	4.0
N vi	1.4×10^{17}	3.0
N vii	2.4×10^{17}	4.0
O vii	7.6×10^{17}	4.0
O viii	7.9×10^{17}	6.0
Ne ix	4.6×10^{17}	4.0 ^a
Ne x	4.7×10^{17}	4.0 ^a
Mg xi	2.2×10^{17}	4.0 ^a
Mg xii	4.0×10^{17}	4.0 ^a
Si xiii	6.2×10^{17}	4.0 ^a
Si xiv	1.1×10^{18}	4.0 ^a

^aUnconstrained parameter. Value fixed at the value used in Kinkhabwala et al. (2002).

L-shell lines. Typically the ionic iron column densities are of the order of about a few times 10^{16} cm^{-2} .

Both the velocity measurements are in reasonable agreement with the average linewidths and line shifts measured from the individual

line centroid energies. Kinkhabwala et al. (2002) quote, based on the NGC 1068 data, an estimate for the uncertainties on the individual model parameters of approximately a few tens of per cent for the ionic column densities and approximately a factor of 2 for the transverse and radial velocities. Here, the data are of somewhat worse statistical quality than the NGC 1068 spectra and so we expect the parameters to be less well constrained. NGC 1068 is a factor of ~ 3 times brighter than NGC 4151 and hence the errors on the fitting parameters from the NGC 4151 spectrum will be a factor of ~ 2 times greater than the errors estimated for the NGC 1068 fitting parameters. Using a fractional ionic abundance of 0.5 for O viii, the column density of O vii quoted in Table 4 yields an equivalent hydrogen column density of $N_{\text{H}} \gtrsim 2 \times 10^{21} \text{ cm}^{-2}$.

4 A COMPARISON WITH NGC 1068 AND MRK 3

The archetypal type 2 Seyfert galaxies NGC 1068 and Mrk 3 have both been the targets of recent X-ray grating observations. The soft X-ray emission in both of these sources is extremely similar to the soft X-ray emission from NGC 4151; it is extended on scales of hundreds of parsecs, shows a strong correlation with the optical ionization cones identified in *HST* [O III] ($\lambda 5007$) images (Sako et al. 2000; Young et al. 2001) and the soft X-ray spectra are all dominated by similar emission lines and RRC.

4.1 The comparison with the *XMM-Newton* RGS spectrum of NGC 1068

The soft X-ray *XMM-Newton* RGS spectrum of NGC 4151 is remarkably similar to that of NGC 1068. Both sources show strong hydrogen-like and helium-like line emission and RRC from carbon, nitrogen, oxygen, neon, magnesium and silicon. The resemblance between the spectra is apparent in the details of the spectra as well as on a more general level. For example, both sources show similar patterns of resonance, intercombination and forbidden linestrengths for the helium-like triplets of nitrogen and oxygen and both show significant (but unresolved) iron L-shell emission. The properties of the detected emission lines are remarkably alike in the two sources, in terms of both the lines present and the scale of their energy shifts. In both sources the prominent emission lines are blueshifted by $< 1000 \text{ km s}^{-1}$ with average line shifts of 305 and 375 km s^{-1} for NGC 4151 and 1068, respectively (Kinkhabwala et al. 2002). The linewidths measured for NGC 1068 do not show the bimodal distribution observed in NGC 4151. However, since only seven lines have constrained linewidths in the NGC 4151 spectrum, compared to 23 lines with constrained widths in the NGC 1068 spectrum, caution should be strongly emphasized in interpreting the validity of the distribution of linewidths in NGC 4151. Interestingly the average linewidth found in the NGC 1068 data ($\sim 1100 \text{ km s}^{-1}$ FWHM) is comparable to the average linewidth of the group of broader lines in the NGC 4151 spectrum ($\sim 1000 \text{ km s}^{-1}$ FWHM). It is tempting, based upon a comparison of the helium-like triplet plasma diagnostic ratios (R and G ; Section 3.3) to infer that the ionization cones in NGC 4151 have a somewhat lower electron temperature and a somewhat higher electron density than those in NGC 1068 (Kinkhabwala et al. 2002). Unfortunately, the situation may not be as clear cut as this simple comparison suggests, primarily due to the unknown effect of photoexcitation on the diagnostic ratios (discussed previously in Section 3.3). The best-fitting ionic column densities for NGC 1068 were found to be similar to those observed *in absorption* for type 1 Seyfert galaxies, implying either radially stratified ionization zones or, more likely, a broad distribution of densities at any given radius. An inspection of the radial column densities fitted to the RGS spectrum reveals that NGC 4151 appears to have less ionized material in its ionization cones, by a factor of ~ 3.5 on average. The best-fitting ionic electron temperatures, based on the widths of the RRC features, are also extremely similar between NGC 4151 and 1068 (although the comparatively large errors on these temperatures prevents any definite conclusions being drawn regarding this similarity). The ionic column densities are dependent on a combination of factors including cone length, density, ionization parameter and the filling factor of the material. Lower ionic column densities could be the result of lower ionizing flux or less material in the ionization cones. However, a somewhat more plausible explanation, in line with the smaller R -values from the helium-like line triplets, could be that the material in the ionization cones of NGC 4151 is rather more dense than the material in the ionization cones of NGC 1068. Since the recombination rate is dependent on the density of the material, this can result in a smaller ionized fraction for a similar ionizing continuum.

4.2 The comparison with the *Chandra* HETG observation of Mrk 3

The *Chandra* HETG observation of Mrk 3 was the first published high-resolution soft X-ray spectrum of a type 2 Seyfert galaxy and showed unambiguously that the soft X-ray emission in Mrk 3 is composed almost entirely of emission lines and RRC, with little or

no continuum emission. The soft X-ray spectrum of Mrk 3 is, again, remarkably analogous to the soft X-ray spectrum of NGC 4151, though with somewhat less statistical significance due to the rapidly decreasing effective area of the HETG instrument at wavelengths above $\sim 9 \text{ \AA}$. In both sources there is strong evidence to suggest that the observed emission lines are produced in a photoionized and photoexcited plasma (Sako et al. 2000). The importance of photoexcitation in the spectrum of Mrk 3 is highlighted by the observed weak iron L-shell emission, rather than by the enhanced higher-order resonance transitions, rejecting explanations from a recombination- or collisionally dominated plasma. Despite this impressive spectrum, the *Chandra* observation of Mrk 3 only partially resolves two of the helium-like line triplets detected in the RGS spectrum of NGC 4151 (oxygen and neon), because of the limited number of photons in each feature, and as a result many of the properties of the plasma are not well constrained. In particular, the resonance and intercombination lines of these triplets cannot be separated and as a result Sako et al. (2000) quote a different diagnostic line ratio, i.e. $(r + i)/f$, from the line ratios used here.

At wavelengths shorter than $\sim 9 \text{ \AA}$, the *Chandra* spectrum shows evidence for a reflection-dominated continuum along with clear detections of emission lines that are either extremely difficult or impossible to detect with the RGS (given its limited spectral bandpass), namely Fe xxvi, Fe xxv, Fe $K\alpha$, S xvi, S xv, S $K\alpha$, Si xiv, Si xiii, Si $K\alpha$, Mg xii and Mg xi (Sako et al. 2000). This plethora of lines highlights the complementary capabilities of *XMM-Newton* and *Chandra* and strongly supports future observations of bright, heavily obscured AGN with both *Chandra* (using the HETG) and *XMM-Newton*, to obtain the highest possible resolution X-ray spectra over the widest possible energy range. The line ratios calculated from the *Chandra* detections of the helium-like silicon and magnesium line triplets (i.e. Si xiii and Mg xi) are all inconsistent with the expected values for a collisionally ionized plasma and are marginally consistent with the predictions from a photoionized plasma, similar to the conclusions from the triplet ratios for both NGC 4151 and 1068.

5 A BRIEF COMPARISON WITH THE *XMM-NEWTON* EPIC SPECTRA

One of the strengths of *XMM-Newton* is that all the science instruments operate simultaneously during each observation, allowing a direct comparison between the high-resolution spectra from the RGS instruments and the lower-resolution spectra from the EPIC CCD detectors. This comparison is particularly useful in exposing features in each source spectrum that the other detectors struggle to detect. For example, broad features present in the 0.3–2.5 keV range are not easily identified in RGS spectra, but will be more clearly observed by the EPIC instruments. Conversely, features that appear to be broad in the EPIC spectrum may be resolved into a set of individual narrow lines by the RGS instruments. Conclusions from the process of comparing the EPIC and RGS spectra are complicated by the need for good calibration *and cross-calibration* for each instrument involved.

Fig. 4 shows the full-window mode EPIC PN spectra fitted with a model that combines the best fit of the hard X-ray model developed in Schurch et al. (2003) and the best fit of the ‘ionization cone’ soft X-ray model presented in Section 3.4. In addition to the hard X-ray model and the ionization cone model, a silicon $K\alpha$ line was included in the fitting. The energy of the line was fixed at 1.73 keV and the linewidth was fixed to be the same width as the iron $K\alpha$ linewidth. The line flux was fixed to be 5 per cent of the flux contained in the

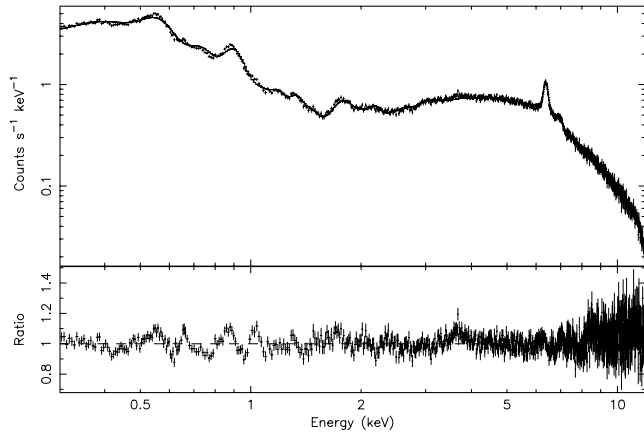


Figure 4. Upper panel: the 0.3–12 keV EPIC PN spectra of NGC 4151 modelled by a combination of the hard X-ray model developed in Schurch et al. (2003) and the ‘ionization cone’ soft X-ray model presented in Section 3.4. Lower panel: the ratio of the data to the model prediction.

iron $K\alpha$ line, in keeping with the ratio of the iron $K\alpha$ to silicon $K\alpha$ line fluxes measured in the high-resolution *Chandra* spectrum of Mrk 3. Initially the column densities of the hydrogen- and helium-like atomic species were fixed to be the values measured by the RGS data. Key parameters in the hard X-ray model (e.g. ionization parameter, iron $K\alpha$ line flux, etc.; see Schurch et al. 2003 for details) were free parameters in the fit, but no contributions from iron L-shell transitions were included in the fit. This highly restricted model does not provide a good fit to the EPIC spectrum, with considerable residuals remaining below 2 keV. Relaxing the constraints of the model by incorporating a contribution from iron L-shell emission improves the fit considerably and results in similar values for the column densities of iron ionization states from Fe XVI–XXIII to those found with the RGS. Despite the improvement, the overall fit remains poor, with considerable residuals still remaining across the soft X-ray region. Relaxing the constraints of the model more considerably by allowing the column densities of the hydrogen- and helium-like atomic species to be free parameters in the model fit provides a reasonable fit to the broad-band X-ray spectrum of NGC 4151 ($\chi^2 = 2709$ for 2194 degrees of freedom); however, residuals remain in the fit below 2 keV at a level of ~ 10 per cent (Fig. 4). The best-fitting column densities for the hydrogen- and helium-like atomic species are typically within a factor of ~ 3 of the best-fitting column densities determined from the RGS modelling. We do not quote these values here because the relatively poor spectral resolution of the EPIC instruments results in considerable degeneracy between the column densities measured for specific atomic species, making any specific values at best unreliable and at worst misleading. Despite this caveat, we note that the best-fitting column densities of N VII, Ne X and Si XIV measured in the EPIC data are considerably lower in comparison with those measured in the RGS data (factors of 3.5, 40 and 16 respectively). The modelling is not significantly improved by the addition of either a soft X-ray power law (representing a scattered fraction of the underlying continuum) or blackbody emission (to represent the canonical ‘soft X-ray excess’ often observed in type 1 Seyfert galaxies). Considerably more detailed modelling of the RGS spectrum utilizing the additional data from the most recent *XMM-Newton* observations of NGC 4151, coupled with improvements in the relative instrument calibrations, is required before any firm conclusions on the nature of the remaining fitting residuals can be determined.

6 SYNOPSIS

We present a detailed analysis of the RGS spectrum of NGC 4151 from a total of ~ 125 ks of *XMM-Newton* observations. The EPIC spectra from these observations are presented in Schurch et al. (2003). The analysis uses the high spectral resolution of the RGS instruments to characterize the nature and origin of the soft X-ray spectrum of NGC 4151.

(i) The soft X-ray spectrum of NGC 4151 (Fig. 1) is completely dominated by line emission and radiative recombination continua. Line emission, including higher-order (β – ϵ) resonance transitions, is clearly detected from hydrogen-like and helium-like ionization states of neon, oxygen, nitrogen and carbon. Much of the unidentified line emission below ~ 16 Å can be associated with a combination of iron L-shell emission and lines from hydrogen-like and helium-like silicon and magnesium.

(ii) The RGS spectra show no significant continuum emission and no fluorescent line emission associated with neutral material.

(iii) The measured line centroid energies are consistent with a blueshift of between ~ 100 and 1000 km s $^{-1}$, with respect to the systemic velocity of NGC 4151. The seven observed linewidths that are constrained by the data tentatively suggest a bimodal distribution, with average linewidths of ~ 1000 and ~ 200 km s $^{-1}$ (FWHM). The measured line blueshifts are generally consistent with the outflow velocities of the absorption lines observed in the UV spectrum of NGC 4151 (Kriss et al. 1995), implying that the UV and X-ray line features originate in the same material.

(iv) Plasma diagnostics, based on the ratios of the resonance, intercombination and forbidden lines of the observed helium-like triplets, imply electron temperatures of $\sim (1\text{--}5) \times 10^4$ K and electron densities of $\sim 10^8$ cm $^{-3}$ in nitrogen and oxygen and $\sim 10^{10}$ cm $^{-3}$ in neon (Porquet & Dubau 2000). We note again that the effects of photoexcitation may have a considerable effect on the values of electron temperature and density determined by these diagnostic ratios (see Section 3.3). The wide range of the calculated electron densities is suggestive of either a ‘clumpy’ extended narrow-line region or a region in which the material has grossly non-solar elemental abundances.

(v) The soft X-ray spectrum of NGC 4151 is remarkably similar to the soft X-ray spectrum of NGC 1068 (Kinkhabwala et al. 2002). The correspondence between the two source spectra is evident on the general scale from the strong emission lines and RRC associated with the same ionic species, which dominate the spectra of both sources. The resemblance of the NGC 4151 and 1068 soft X-ray spectra is also apparent in the details of the spectra (i.e. the similar helium-like triplet ratios and RRC temperatures).

(vi) The ‘ionization cone’ model, developed by Kinkhabwala et al. (2002) to model the RGS spectra of NGC 1068, reproduces all of the hydrogen-like and helium-like emission features observed in the soft X-ray spectrum of NGC 4151 *in detail*. The best-fitting radial and transverse velocities of the material in the ionization cones agree well with the blueshift and velocity dispersion measured from the individual line centroid energies, and are similar to the radial and transverse velocities measured from the soft X-ray spectrum of NGC 1068. The individual ionic column densities are somewhat smaller than those measured for NGC 1068, which, in combination with the plasma diagnostic ratios from the helium-like triplets, suggests that the material in the ionization cones of NGC 4151 may be somewhat denser than the material in the ionization cones of NGC 1068.

ACKNOWLEDGMENTS

NJS gratefully acknowledges financial support from PPARC, and NJS and REG also acknowledge the support of NASA grant NAG5-9902. It is a pleasure to thank Keith Arnaud for his help with XSPEC. This work is based on observations obtained with *XMM-Newton*, an ESA science mission with instruments and contributions directly funded by ESA Member States and the USA (NASA). The authors wish to thank the *XMM-Newton* team for the hard work and dedication that underlies the success of the mission. This research has made extensive use of NASA's Astrophysics Data System Abstract Service.

REFERENCES

- Brinkman A. C., Kaastra J. S., van der Meer R. L. J., Kinkhabwala A., Behar E., Kahn S. M., Paerels F. B. S., Sako M., 2002, *A&A*, 396, 761
- Evans I. N., Tsvetanov Z., Kriss G. A., Ford H. C., Caganoff S., Koratkar A. P., 1993, *ApJ*, 417, 82
- Gabriel A. H., Jordan C., 1969, *MNRAS*, 145, 241
- Griffiths R. G., Warwick R. S., Georgantopoulos I., Done C., Smith D. A., 1998, *MNRAS*, 298, 1159
- Gursky H., Kellogg E. M., Leong C., Tananbaum H., Giacconi R., 1971, *ApJ*, 165, L43
- Jansen F. et al., 2001, *A&A*, 365, L1
- Kinkhabwala A. et al., 2002, *ApJ*, 575, 732
- Kriss G. A., Davidsen A. F., Zheng W., Kruk J. W., Espey B. R., 1995, *ApJ*, 454, L7
- Liedahl D. A., 1999, in van Paradijs J., Bleeker J. A. M., eds, *X-Ray Spectroscopy in Astrophysics*. Springer-Verlag, New York, p. 189
- Liedahl D. A., Paerels F., 1996, *ApJ*, 468, L33
- Ogle P. M., Marshall H. L., Lee J. C., Canizares C. R., 2000, *ApJ*, 545, L81
- Ogle P. M., Brookings T., Canizares C. R., Lee J. C., Marshall H. L., 2003, *A&A*, 402, 849
- Perola G. C. et al., 1986, *ApJ*, 306, 508
- Porquet D., Dubau J., 2000, *A&AS*, 143, 495
- Porquet D., Mewe R., Dubau J., Raassen A. J. J., Kaastra J. S., 2002, *A&A*, 376, 1113
- Pradhan A. K., Norcross D. W., Hummer D. G., 1981, *ApJ*, 246, 1031
- Sako M., Kahn S. M., Paerels F., Liedahl D. A., 2000, *ApJ*, 543, L115
- Sambruna R. M., Brandt W. N., Chartas G., Netzer H., Kaspi S., Garmire G. P., Nousek J. A., Weaver K. A., 2001, *ApJ*, 546, L9
- Schurch N. J., Warwick R. S., Griffiths R. E., Sembay S., Ptak A. F., 2003, *MNRAS*, 345, 423
- Vainshtein L. A., Safronova U. I., 1978, *Atomic Data Nucl. Data Tables*, 21, 49
- Warwick R. S., Done C., Smith D. A., 1995, *MNRAS*, 275, 1003
- Weaver K. A., Yaqoob T., Holt S. S., Mushotzky R. F., Matsuoka M., Yamauchi M., 1994, *ApJ*, 436, 27
- Weisskopf M. C., Brinkman B., Canizares C., Garmire G., Murray S., Van Speybroeck L. P., 2002, *PASP*, 114, 1
- Yang Y., Wilson A. S., Ferruit P., 2001, *ApJ*, 563, 124
- Young A. J., Wilson A. S., Shopbell P. L., 2001, *ApJ*, 556, 6

This paper has been typeset from a $\text{\TeX}/\text{\LaTeX}$ file prepared by the author.